Pharmaceutical Research, Vol. 26, No. 12, December 2009 (© 2009)
DOI: 10.1007/s11095-009-9981-4

Research Paper

Evaluation of a ^{99m}Tc-Labeled AnnexinA5 Variant for Non-invasive SPECT Imaging of Cell Death in Liver, Spleen and Prostate

Rick Greupink,[1,3] Charles F. Sio,[2] Antwan Ederveen,[1] and Joke Orsel[2]

Received June 13, 2009; accepted September 14, 2009; published online September 25, 2009

Purpose. We investigate radio-labeling and pharmacokinetics of a new AnnexinA5 variant (HYNIC-cys-AnxA5) and then assess its utility for the non-invasive detection of cell death in liver, spleen and prostate.
Methods. AnnexinA5 binds to phosphatidylserine expressed on the surface of apoptotic and necrotic cells. Contrary to other AnnexinA5 variants, the new cys-AnxA5 allows for site-specific conjugation of a hydrazinonicotinamide-maleimide moiety and subsequent radio-labeling with ^{99m}Tc at a position not involved in the AnxA5-phosphatidylserine interaction. Distribution of ^{99m}Tc-HYNIC-cys-AnxA5 was studied in rats, both invasively and via SPECT/CT. Cycloheximide was used to induce cell death in liver and spleen, whereas apoptosis in the prostate was induced by castration.
Results. HYNIC-cys-AnxA5 was efficiently and reproducibly labeled with ^{99m}Tc. Blood clearance of radioactivity after iv-injection was adequately described by a two-compartment model, the renal cortex representing the main site of accumulation. Cycloheximide treatment resulted in increased accumulation of intravenous-injected ^{99m}Tc-HYNIC-cys-AnxA5 in liver and spleen over controls, which correlated well with TUNEL staining for cell death in corresponding tissue sections. However, the increase in TUNEL-positive prostate epithelial cells observed following castration was not paralleled by greater ^{99m}Tc-HYNIC-cys-AnxA5 accumulation.
Conclusion. ^{99m}Tc-HYNIC-cys-AnxA5 appears a suitable tracer for assessment of cell death in liver and spleen, but not prostate.

KEY WORDS: annexinA5; apoptosis; cell death; molecular imaging; SPECT/CT.

INTRODUCTION

Molecular imaging techniques provide a non-invasive means of visualizing physiological processes at the cellular and sub-cellular levels and are an emerging strategy in the *in vivo* pharmacological evaluation of new drugs. Single photon emission computed tomography (SPECT) and positron emission tomography (PET) may be applied to assess pharmacokinetics and *in vivo* receptor binding of radio-labeled drugs and can also be used for measurement of target modulation when applied in combination with appropriate molecular probes. Due to their application to human studies, nuclear imaging assessments can provide relevant clinical information at an early stage during drug development, assist in the generation of data, which can be translated from pre-clinical research to clinical development, and potentially provide surrogate endpoints in clinical trials. Applying a non-invasive longitudinal scan approach in pre-clinical pharmacological research may also contribute to a reduction in the use of experimental animals (1–3).

This study characterizes the use of a novel molecular imaging probe and non-invasive imaging to investigate cell death. Many drugs exert their beneficial effect via the induction of apoptosis. Moreover, drug-induced side-effects can be the result of excessive apoptosis or necrosis occurring in non-target tissues. In previous studies, annexin A5 (AnxA5) has been described as a molecular probe for the imaging of cell death by virtue of its selective binding to phosphatidylserine (PS) residues that are expressed on the cell membrane of apoptotic and necrotic cells (4–6). Recently, a novel AnxA5 variant has been developed by Reutelingsperger and collaborators which allows specific radio-labeling of the protein with ^{99m}Tc at a site which is remote from the domains involved in the interaction of AnxA5 with PS (7). In principle, labeling should therefore not negatively influence the capability of AnxA5 to bind PS on target cells.

Here, the utility of this second generation cys-AnxA5 for the non-invasive detection of cell death is investigated in the rat for the first time. First, we study the feasibility of imaging

[1] Schering-Plough Research Institute, Oss, The Netherlands.
[2] Department of Biomolecular Engineering, Philips Research, Eindhoven, The Netherlands.
[3] To whom correspondence should be addressed. (e-mail: rick.greupink@spcorp.com)

ABBREVIATIONS: AnxA5, AnnexinA5; Cys-AnxA5, AnnexinA5 with cysteine incorporated via site-directed mutagenesis; HYNIC, Hydrazinonicotinamide; ORX, Orchiectomy; PS, Phosphatidylserine; ROI, Region of interest; SEM, Standard Error of the Mean; SPECT/CT, Single Photon Emission Computed Tomography/Computed Tomography; TUNEL, Terminal deoxynucleotidyl transferase dUTP Nick End Labeling; %ID, Percentage of Injected Dose.

cycloheximide-induced cell death in liver and spleen with the cys-AnxA5 variant and correlate this to apoptosis determined via traditional histological methods. From a drug discovery perspective, these studies have value in themselves, given the central role cell death plays in a number of diseases that affect these organs and their respective experimental therapies (8–10). At the same time, the studies in liver and spleen form a step-up to our main aim, which is to explore translational strategies to assess drug-induced apoptosis in prostates, in order to expedite the development of new drugs to treat prostate cancer and benign prostate hyperplasia. We therefore tested whether this novel annexin variant can be used to appraise apoptosis in the rat prostate.

In the current paper, the radiochemical labeling of HYNIC-cys-AnxA5 with ^{99m}Tc is described, and the evaluation of the tracer in detecting cell death in liver, spleen and prostate is discussed in relation to its pharmacokinetic and physicochemical properties.

MATERIALS AND METHODS

^{99m}Tc Labeling of Annexin A5

^{99m}Tc-labeled AnxA5 was freshly prepared immediately prior to each experiment. The novel recombinant hydrazinonicotinamide-cysteine-AnxA5 (HYNIC-cys-AnxA5) was obtained from MosaMedix BV (Kattendijke, The Netherlands) and has been recently described by Reutelingsperger and colleagues (7). The cys-AnxA5 variant used in the present studies contains one native cysteine, which is buried within the 3D structure of the protein, as well as one engineered cysteine residue at the concave side of the protein. The latter is readily accessible for conjugation reactions. In brief, labeling of HYNIC-cys-AnxA5 was performed as follows. In a glass reaction vial, 64 µl of a 30 mg/ml tricine solution in citrate buffer (pH 5.2) was mixed with 14 µl of 0.85 mg/ml $SnCl_2$ in a 0.05 M HCl solution. Under gentle mixing, 100–120 MBq of ^{99m}Tc was added, and the reaction vial was flushed with nitrogen gas. Subsequently, 50 µg of HYNIC-cys-AnxA5 was added to the reaction mixture, and the solution was incubated at room temperature for 15 min under nitrogen atmosphere to allow for effective chelation of ^{99m}Tc to tricine and the HYNIC-cys-AnxA5 conjugate. The resulting reaction mixture was purified via gel filtration, and radiochemical purity was checked via HPLC analysis before and after purification. The HPLC system (Agilent 1200 series) was fitted with a Biosep-SEC-S 03C-2146-K0 guard column (Phenomenex, Utrecht, The Netherlands) and a Biosep-SEC-S-3000 00H-2146-K0 size exclusion analytical column (Phenomenex). The 50 µg of HYNIC-cys-Annexin were labeled with 78 +/− 2.2 MBq ^{99m}Tc (n=24 syntheses), assuming that full protein recovery had taken place after purification. Compounds were separated using a mobile phase of 50 mM phosphate / 150 mM NaCl buffer (pH=6.8) at a flow of 1 ml/min. Eluted products were traced via online gamma detection.

Experimental Animals

Male Wistar rats (Charles River, Kissleg, Germany) of 250–450 g were housed under a 12 h dark/light cycle at constant humidity and temperature. Animals were permitted free access to tap water and standard lab chow. All experiments were approved by the committee for care and use of laboratory animals of the University of Maastricht and were performed according to strict governmental and international guidelines.

SPECT/CT Scanning Protocol

Animals were anesthetized with isoflurane, and the tail vein was canulated for tracer administration. The rats were positioned in the SPECT/CT scanner (NanoSPECT/CT^{TM}, Bioscan Inc.,Washington DC, USA) and were maintained under anesthesia for the duration of the experimental procedure. Body temperature was maintained by heating the animal bed via a continuous flow of warm air, while anesthesia depth was continuously assessed via monitoring of breathing frequency. Maximum anesthesia time was 4 h in all experiments described. The NanoSPECT/CT^{TM} used in the present studies is a multi-pinhole SPECT/CT system that consists of four detectors, each with a 9-pinhole collimator. The diameter of the pinholes is 2.5 mm, and the scanning mode is helical for both SPECT and CT.

Prior to tracer injection, a CT-scan was obtained to enable anatomical co-registration. The CT-scan was made with a tube voltage of 65 kV and an exposure time of 2000 msec. Measurements were obtained over 360 projections, and total CT-scan time was 12 min. After completion of the CT scan, ^{99m}Tc-HYNIC-cys-AnxA5 was injected and 3D SPECT images were obtained to quantify the distribution of the injected tracer. SPECT measurements were taken at various time points after injection. ^{99m}Tc was detected at 140 keV with a 20% energy window. For SPECT and CT image fusion, data analysis and quantification of ^{99m}Tc-labelled annexin distribution and accumulation over time the InVivo Scope software package was used. Liver, spleen, ventricles of the heart and prostate were identified in the reconstructed CT images, which allowed Region of Interest (ROI) determination for analysis of tracer levels in these organs. When defining the prostate ROI, particular care was taken to avoid inclusion of any erroneous signal originating from the bladder. The average radioactivity in the selected ROI was subsequently expressed as the percentage of injected dose present per cm^3 of ROI, simultaneously correcting values for animal weight.

Pharmacokinetics After I.V. Injection

First, the overall body distribution and plasma pharmacokinetics of radioactivity after i.v. injection of ^{99m}Tc-HYNIC-cys-AnxA5 were determined in the healthy rat. Sequential SPECT scans of 5 min duration were acquired of the thorax after injection of a single tracer dose of 50 MBq, equivalent to approximately 30 µg of ^{99m}Tc-HYNIC-cys-AnxA5. Based on a CT image of the thorax, a region of interest was defined that corresponds to the ventricles of the heart, in order to measure clearance of radioactivity from the central compartment. Pharmacokinetic parameters were subsequently derived as described previously, using non-linear curve fitting software (11). At the end of these measurements a whole-body SPECT

scan was obtained to assess the overall levels of activity throughout the body.

Apoptosis in Liver and Spleen

Male rats underwent a ^{99m}Tc-Annexin SPECT baseline scan as described above and were allowed to recover for three days. After this period, a 5 mg/kg i.p. dose of cycloheximide in saline or saline alone was injected 2 h prior to a second i.v. injection of ^{99m}Tc-HYNIC-cys-AnxA5 and the conduction of a second SPECT scan series. Animals were maintained under isoflurane anesthesia for the complete duration of the experiment. Three SPECT scans of 15 min scan time were collected of the liver and spleen area. Following completion of the SPECT scans, the animals were sacrificed, and blood and tissue samples were removed to determine radioactivity in each organ and for histochemical assessment of apoptosis via TUNEL staining.

Apoptosis in the Ventral Prostate of Castrated Rats

To determine at which timepoint after orchiectomy (ORX) apoptosis in the ventral rat prostate was maximal, rats were surgically castrated according to standard procedures. One, three and seven days after ORX, groups of 3–4 animals were sacrificed, and the ventral prostate was excised for histochemical analysis of apoptotic cell death (TUNEL staining, procedure see below). In subsequent non-invasive studies, rats were submitted to a baseline SPECT/CT scan with ^{99m}Tc-HYNIC-cys-AnxA5 before being submitted to ORX (for a detailed description of the scan protocol, see paragraph above). After the baseline scan, the animals were castrated, and rats were allowed to recover for three days before the second scan (the time-point determined in the histochemical studies to display maximum levels of apoptosis). At the end of the second scan, animals were sacrificed via cervical dislocation, and tissues and blood were removed to determine levels of ^{99m}Tc in each organ and for histochemical detection of apoptosis via TUNEL staining.

TUNEL Staining

Detection of apoptotic cells was performed via Terminal deoxynucleotidyl Transferase dUTP nick end labeling (TUNEL). Tissues were fixed in 4% formalin and embedded in paraffin. After deparaffinization, 4 µm sections were incubated in DNAse-free proteinase K (20 µg/ml, Promega Benelux, Leiden, The Netherlands). Endogenous peroxidase activity was blocked via incubation in methanol containing 0.3% H_2O_2. Tissues were then incubated with TdT reaction mix (Biotin dUTP from Roche, Almere, The Netherlands and TdT enzyme from Promega) for 2 h at 37°C. Bound Biotin-labeled dUTP was demonstrated via incubation with avidin-biotin-peroxidase complex (Vectastain ABCkit, Vector, Burlingame, USA) followed by incubation with diaminobenzidine obtained from Pierce, via Perbio Science, Etten-Leur, The Netherlands. Tissue sections were embedded in mounting medium and were evaluated with a Leica DM6000B microscope fitted with a Leica DFC420C camera, using the Leica Application Suite V3.0.0 software package.

Post-mortem Assessment of Biodistribution

Accumulation of ^{99m}Tc-labelled annexin in various tissues was also assessed post-mortem using a 1480 Wizard™ 3" gamma counter (Perkin Elmer, Waltham, MA, USA). Activity data were corrected for radioactive decay of ^{99m}Tc and re-calculated to reflect activity at time of injection

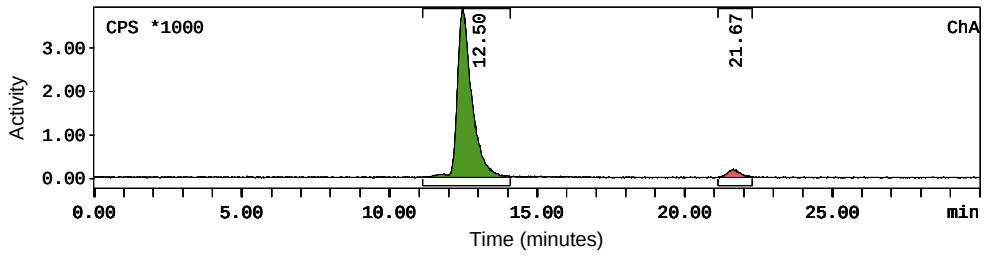

A

Compound	R/T min
Annexin-hynic-TC99m	12.50
Tricine-Tc	14.20
Pertechnetate	21.67

B

n = 24 syntheses	*Amount of bound and unbound technetium in the preparation (% of total Tc content)*		
	Annexin-bound	**Only Tricine-bound**	**Pertechnetate**
Before purification	92.3 ± 1.4 %	6.5 ± 1.0 %	1.9 ± 0.7 %
After purification	97.5 ± 0.5 % *	0.04 ± 0.06 % *	2.4 ± 0.5 %^{NS}

Fig. 1. A Typical example of an HPLC radiochromatogram of ^{99m}Tc-HYNIC-cys-AnxA5, after purification of the reaction mixture. Eluted compounds were detected via an online gamma counter. **B** Percentages of total ^{99m}Tc bound to annexin, only bound to tricine or present in free form. Data are expressed as mean +/− SEM. * indicates $p<0.05$, NS: not significant compared to pre-purification values.

to allow for comparison of the data to the SPECT scans. Distribution data were then expressed as a percentage of the injected dose, corrected for weight parameters (body weight and organ weight), i.e. %ID×kg body weight / gram of tissue (12).

Statistical Evaluation

Results are expressed as mean±Standard Error of the Mean (SEM). When comparing two groups, the data were subjected to the two-sided Student's *t*-test, whereas comparison of multiple groups was performed via one-way analysis of variance, followed by the LSD post-hoc test. Differences were considered statistically significant at the $p<0.05$ level.

RESULTS

Labeling and Characterization of HYNIC-cys-AnxA5

Twenty-four individual labeling procedures were performed, which all resulted in a successful conjugation of ^{99m}Tc to HYNIC-cys-AnxA5, as assessed via HPLC (Fig. 1A). Before purification of the reaction mixture 92.3±1.4 % of ^{99m}Tc was bound to HYNIC-cys-AnxA5, whereas 6.5±1.0 % and 1.9±0.7 % of radioactive technetium was present bound to tricine or present as unbound pertechnetate, respectively. After purification, 97.5±0.5 % of ^{99m}Tc was HYNIC-cys-AnxA5-bound, whereas the tricine-bound ^{99m}Tc and the free pertechnetate fraction accounted for 0.04±0.06 % and 2.4 ± 0.5 %, respectively (Fig. 1B). The ^{99m}Tc-HYNIC-cys-AnxA5-tricin complex consisted almost completely of the monomeric protein, eluting at 12.50 min. Formation of dimers or polymers during the synthesis procedure was virtually absent. Only the purified product was used in *in vivo* evaluation studies.

Pharmacokinetics After I.V. Injection

Knowledge of tracer pharmacokinetics is a crucial step in the evaluation of a new tracer. We therefore assessed plasma clearance and organ distribution of radioactivity after injection of ^{99m}Tc-labeled HYNIC-cys-AnxA5 in the healthy rat. In Fig. 2A, the disappearance of radioactivity from the central compartment is displayed after a single i.v. injection. The data could be adequately described by a two-compartment model, as assessed by calculation of Akaike's Information Criterion. The calculated parameters are presented in Fig. 2B, assuming a model in which elimination takes place from the central compartment.

In Fig. 3A, a whole body maximum intensity projection is shown of ^{99m}Tc-HYNIC-cys-AnxA5 biodistribution in relation to the anatomical background of the animal. From observation, it is clear that the kidneys are the main organs to which ^{99m}Tc-HYNIC-cys-AnxA5 distributes following i.v.

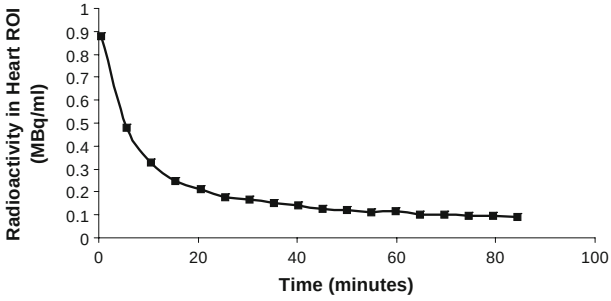

A

parameter	value	unit
$AUC_{0\text{-}84}$	19.4	min*MBq/ml
CL_d	6.4	ml/min
CL	2.3	ml/min
$t_{1/2\ distribution}$	4.9	min
$t_{1/2\ terminal}$	72.3	min

parameter	value	unit
V1	53.7	ml
V2	130.7	ml
Vss	184.4	ml

B

Fig. 2. **A** Clearance of ^{99m}Tc-HYNIC-cys-AnxA5 from the central compartment as defined by a Region of Interest corresponding to the ventricles of the heart. Data was obtained in the healthy rat. **B** Pharmacokinetic parameters derived from the plasma disappearance data. Data were analyzed assuming a two-compartment model, with elimination from the central compartment and an estimated duration of the i.v.-bolus injection of 0.1 min. $t_{1/2\ distribution}$=half-life in distribution phase, $t_{1/2\ terminal}$=terminal half-life, V_1=volume of distribution of virtual compartment 1, V_2=volume of distribution of virtual compartment 2, CL_d=distribution clearance, CL=clearance, V_{ss}=volume of distribution at steady state, AUC=area under the curve (as calculated from model function).

injection, and that much lower levels of ^{99m}Tc-HYNIC-cys-AnxA5 accumulate in spleen and liver. These non-invasive observations were confirmed by analysis of the reconstructed SPECT data and by subsequent post-mortem analysis (Fig. 3B). Further analysis of the SPECT/CT data demonstrated that renal uptake is mainly confined to the renal cortex (Fig. 3C). Moreover, from a time-course analysis, it is clear that accumulation in the kidney is rapid and remains constant for at least up to 120 min after injection (Fig. 3D).

Detection of Apoptosis in Liver and Spleen

First, we investigated the functionality of ^{99m}Tc-HYNIC-cys-AnxA5 *in vivo* in a cycloheximide-induced animal model of liver and spleen injury. Analysis of TUNEL-stained sections confirmed that a clear increase in the number of TUNEL-positive cells was present in both organs, 2 h following an i.p. injection of cycloheximide. In the spleen, the TUNEL-positive cells were mainly macrophages present within the red-pulp. In the liver, an increase in TUNEL-positive sinusoidal cells could be identified, most likely to be Kupffer cells (Fig. 4).

The increase in cell death observed using TUNEL histochemistry correlated with the changes observed in annexin biodistribution as measured via SPECT. First, animals were submitted to a baseline scan in which the uptake of ^{99m}Tc-HYNIC-cys-AnxA5 was determined in liver and spleen of naive animals. Following this, rats were allowed to recover for 3 days and were subsequently administered cycloheximide or vehicle. Two hours following cycloheximide or vehicle administration, the distribution and levels of ^{99m}Tc-HYNIC-cys-AnxA5 were investigated via SPECT/CT imaging. When compared to either vehicle injection or baseline scans, administration of cycloheximide led to an approximate 2-fold and 4-fold increase in accumulation of ^{99m}Tc-HYNIC-cys-AnxA5 in liver and spleen, respectively, within 15 min after ^{99m}Tc-HYNIC-cys-AnxA5 injection (Fig. 5A–B).

This difference in ^{99m}Tc-HYNIC-cys-AnxA5 distribution is also illustrated in Fig. 5C, in which the maximum intensity projections of the abdomen of a cycloheximide- and vehicle-injected rat are shown. The data obtained using non-invasive SPECT scans of annexin biodistribution demonstrated a good correlation to the data obtained from tissues excised at the end of the experiment (Fig. 5D).

Detection of Apoptosis in Ventral Rat Prostate

Next, studies in orchiectomized rats were performed to investigate the potential applicability of ^{99m}Tc-HYNIC-cys-

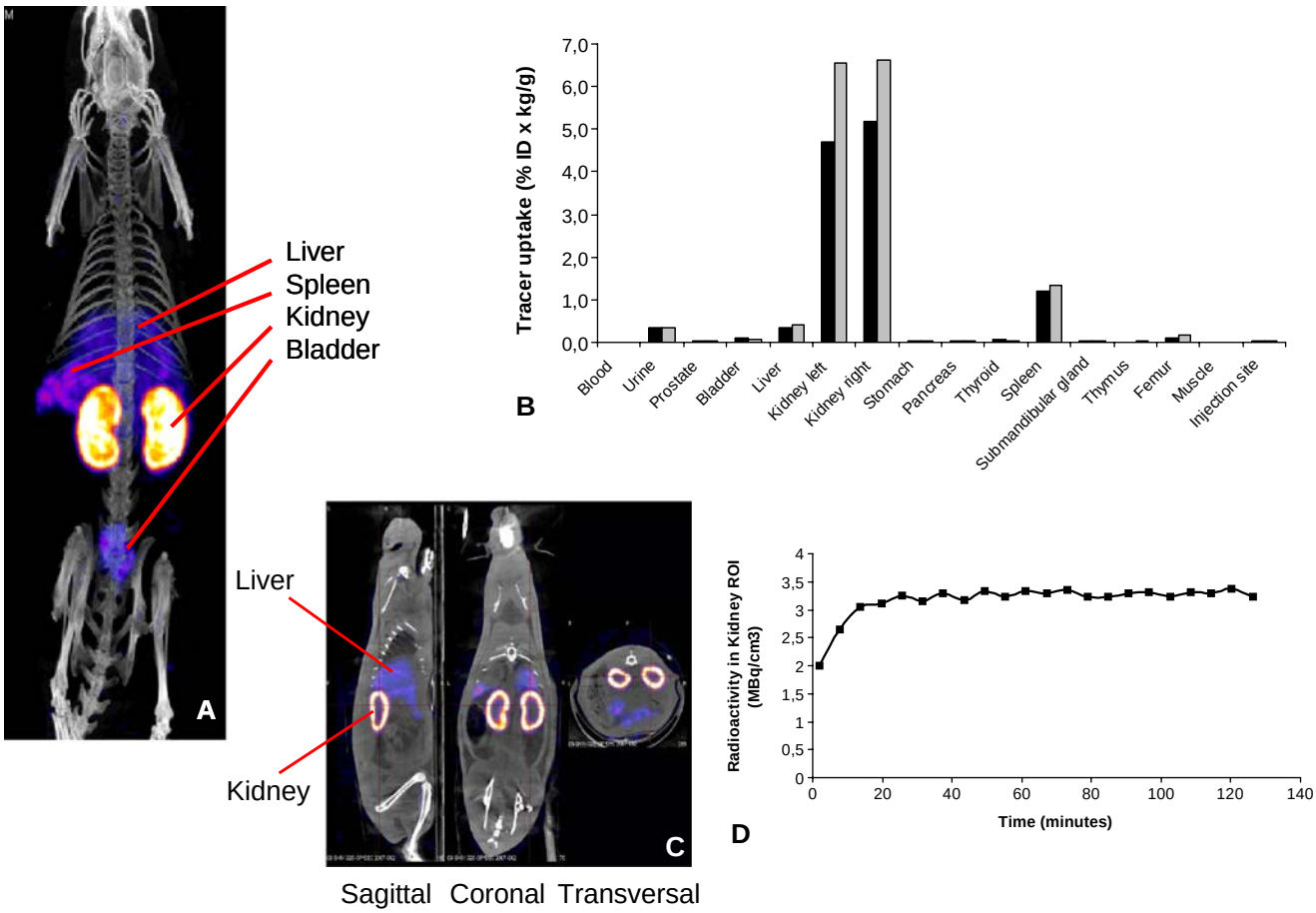

Fig. 3. **A** Maximum intensity projection of a co-registered SPECT and CT image of ^{99m}Tc-annexin biodistribution in the rat 210 min after i.v. injection. **B** Post-mortem assessment of annexin biodistribution (n=2). Individual values of both animals are shown. **C** Sagittal, transversal and coronal slices of SPECT/CT images, clearly showing intra-organ distribution of ^{99m}Tc-HYNIC-cys-AnxA5 within the kidney. **D** Typical example of the kinetics of the renal accumulation of ^{99m}Tc-HYNIC-cys-AnxA5 over time. Data were obtained in healthy animals.

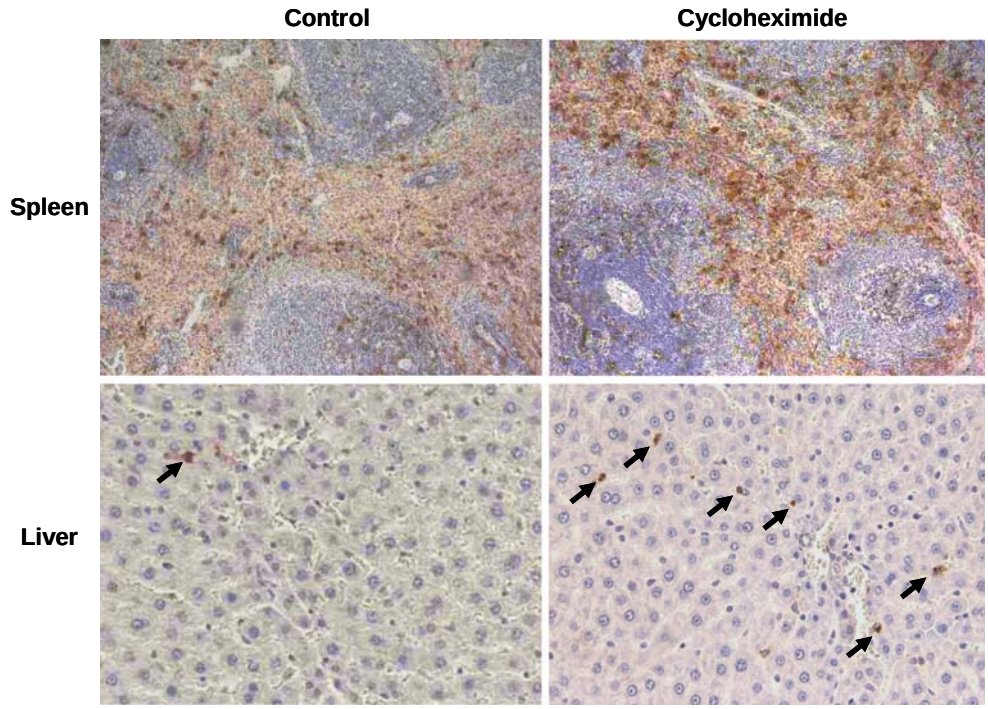

Fig. 4. Representative microphotographs of TUNEL-stained sections of liver and spleen. Note the increase in TUNEL-positive cells after cycloheximide administration in both organs, especially spleen (*brown staining*). In liver, arrows help indicating TUNEL-positive cells. Tissues were obtained approximately 210 min after injection of cycloheximide or vehicle. Original magnification: Spleen 200×, Liver 400×.

AnxA5 for imaging of cell death in the prostate. Castration results in a decrease in systemic testosterone levels, which in turn leads to loss of prostate epithelial cells via apoptosis. Before performing any SPECT studies of the prostate, we first determined at which time-point after castration apoptosis is most prominent. In Fig. 6A representative microphotographs of TUNEL-stained sections of prostate tissue from an intact rat and a castrated rat are shown. Apoptotic indices amounted to 0.6±0.1 % in control rats and to 5.2±0.6 %, 6.8±0.9 % and 5.2±0.8 % at 1, 3 and 7 days post castration, respectively (Fig. 6B). Therefore, the 3-day time-point was chosen for the evaluation of the non-invasive imaging approach. Although stromal cells were also occasionally TUNEL-positive, staining was mainly seen in prostate epithelial cells.

Despite the strong increase of epithelial cell death in the prostate to a high absolute apoptotic index at 3 days after castration, in the SPECT studies, no significant increase in accumulation of ^{99m}Tc-HYNIC-cys-AnxA5 could be seen in the prostates of castrated animals for at least 90 min after injection (Fig. 6C). This was confirmed in excised tissues (Fig. 6D).

DISCUSSION

In the present paper, we demonstrate that the AnxA5 variant under investigation can be reproducibly labeled with ^{99m}Tc to high radiochemical purity and adequate specific activity which allows imaging via combined SPECT/CT. Kinetics of plasma disappearance and renal uptake of this annexin variant were not reported before. With regard to this, we now demonstrated that in the healthy rat, ^{99m}Tc-HYNIC-cys-AnxA5 is cleared very rapidly from the circulation in the initial phase after injection and that the rapid distribution to kidneys, and to a smaller extent liver and spleen, is predominantly responsible for the rapid decline of tracer concentration in the central compartment. The slow second phase of plasma clearance probably reflects redistribution of intact annexin or its radio-labeled metabolites from the tissues back to the central compartment.

The kidney is the main organ to which the tracer distributes and, within this organ, we could demonstrate that the activity was concentrated in the renal cortex. This is in line with the biodistribution of other annexin variants (13–15) as well as with the distribution of other low molecular weight proteins, such as lysozyme, aprotinin and cytochrome c (16). Uptake into the renal cortex is thus considered to be apoptosis-independent and is likely to be mediated via initial glomerular filtration and subsequent re-uptake through high capacity / low specificity transport, for instance via Megalin receptors present in the luminal membrane of proximal tubular epithelial cells (17). Having been reabsorbed back from the ultrafiltrate into proximal tubule cells, proteins are generally routed to the lysosomes for proteolytical degradation (16,18). Degradation products can then either be reabsorbed into the circulation at the basal membrane of the proximal tubule cell, or can be secreted into the urine via the luminal membrane. In line with lysosomal degradation taking place, HPLC analysis of urine obtained via bladder puncture at the end of the experiments revealed that no intact ^{99m}Tc-labeled annexin was present in the urine (data not shown). Besides uptake in the kidneys, we also observed some accumulation of the tracer in the liver and spleen of healthy animals. Studies by Tait *et al.* indicate this is the combined result of basal apoptotic levels within these organs,

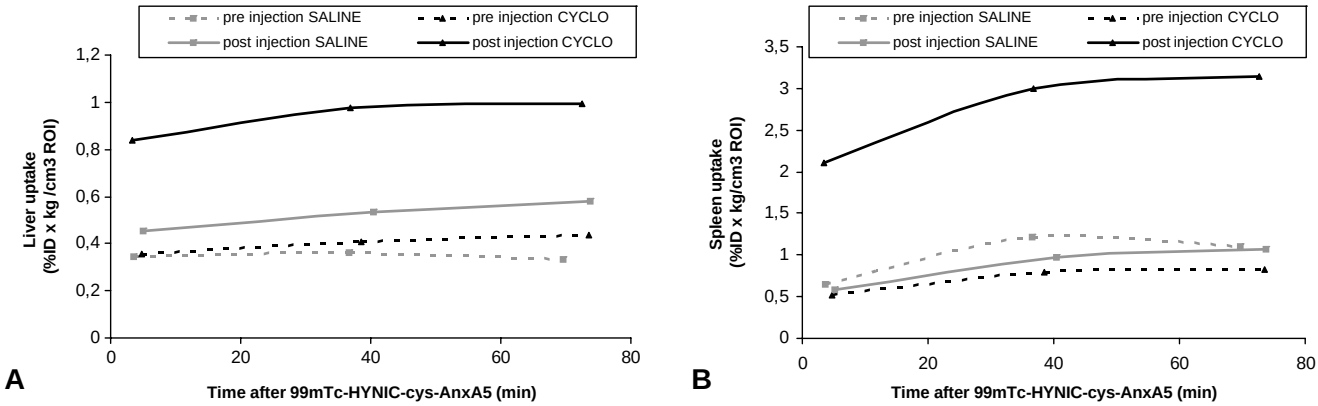

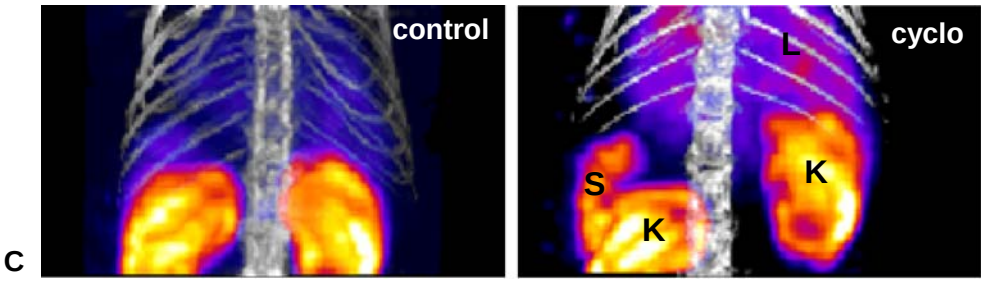

Post-mortem analysis	Uptake in liver (%ID x kg/g)	Uptake in spleen (%ID x kg/g)	Activity in blood (%ID x kg/g)	Liver:blood ratio	Spleen:blood ratio
Control	0.71	3.12	0.09	8	35
Cycloheximide-treated	1.08	5.24	0.04	27	131

D

Fig. 5. Quantification of the accumulation of ^{99m}Tc-HYNIC-cys-AnxA5 in liver (***A)*** and spleen (**B)** obtained via SPECT/CT. Dotted lines represent scan data obtained from single animals prior to injection of saline (*grey*) cycloheximide (*black*). Solid lines represent data obtained from same animals but now after saline (*grey*) or cycloheximide (*black*). **C** Maximum intensity projection of the abdomen of a vehicle- or cycloheximide-treated rat. Note the increase in ^{99m}Tc-HYNIC-cys-AnxA5 accumulation in liver and spleen after cycloheximide treatment. S indicates spleen, L indicates liver, K indicates kidneys. **D** Post-mortem assessment of annexin biodistribution to liver and spleen 120 min after injection of the tracer.

as well as due to a non-specific uptake process (19). Presumably, the latter is due to processing of AnxA5 by cells of the reticulo-endothelial system situated in these organs.

Our data show that the increased accumulation of ^{99m}Tc-HYNIC-cys-AnxA5 in rat liver and spleen after exposure to cycloheximide corresponds to the increased number of TUNEL-positive cells found within these organs. These findings expand the data of Fonge *et al.*, who showed that ^{99m}Tc-HYNIC-cys-AnxA5 can be used to demonstrate cell death in the liver of mice treated with FAS-activating antibody and myocardial infarction-reperfusion injury in rabbits (7). With regard to drug discovery, non-invasive *in vivo* imaging of the PS-Cys-AnxA5 interaction in liver and spleen can provide a relevant translational biomarker to measure early effects of drugs designed to intervene in diseases that affect these organ systems.

Examples comprise diseases in which cell death plays an important role in the pathology and for which novel therapies aim to induce or inhibit cell death from occurring. In this respect, annexin-imaging could provide an interesting biomarker when evaluating new treatments for primary or secondary liver cancer. Yet, the approach may also aid in the evaluation of antifibrotic drugs that aim to induce apoptosis in the populations of liver fibroblasts responsible for the excessive production of collagens that characterize this disease (9,20). Finally, imaging of the PS-Cys-AnxA5 interaction may be applied to study the undesired induction of cell death by drugs in the liver and spleen in more detail. Hepatotoxicity is a common reason for termination of the development process for a new drug, whereas loss of cellularity in a primary lymphoid tissue such as the spleen has also been described (21–24). In exploratory toxicology, the annexin-approach could thus be applied to study onset and reversal of cell death after the respective start and cessation of therapy in a single animal. In contrast, traditional histological evaluation of tissue sections would require much larger numbers of experimental animals in order to obtain the same information.

Although the use of older AnxA5 variants for detection of cell death in organs such as heart, liver and certain tumors has been documented before, only little is known about the non-invasive imaging of apoptosis with any AnxA5 variant in

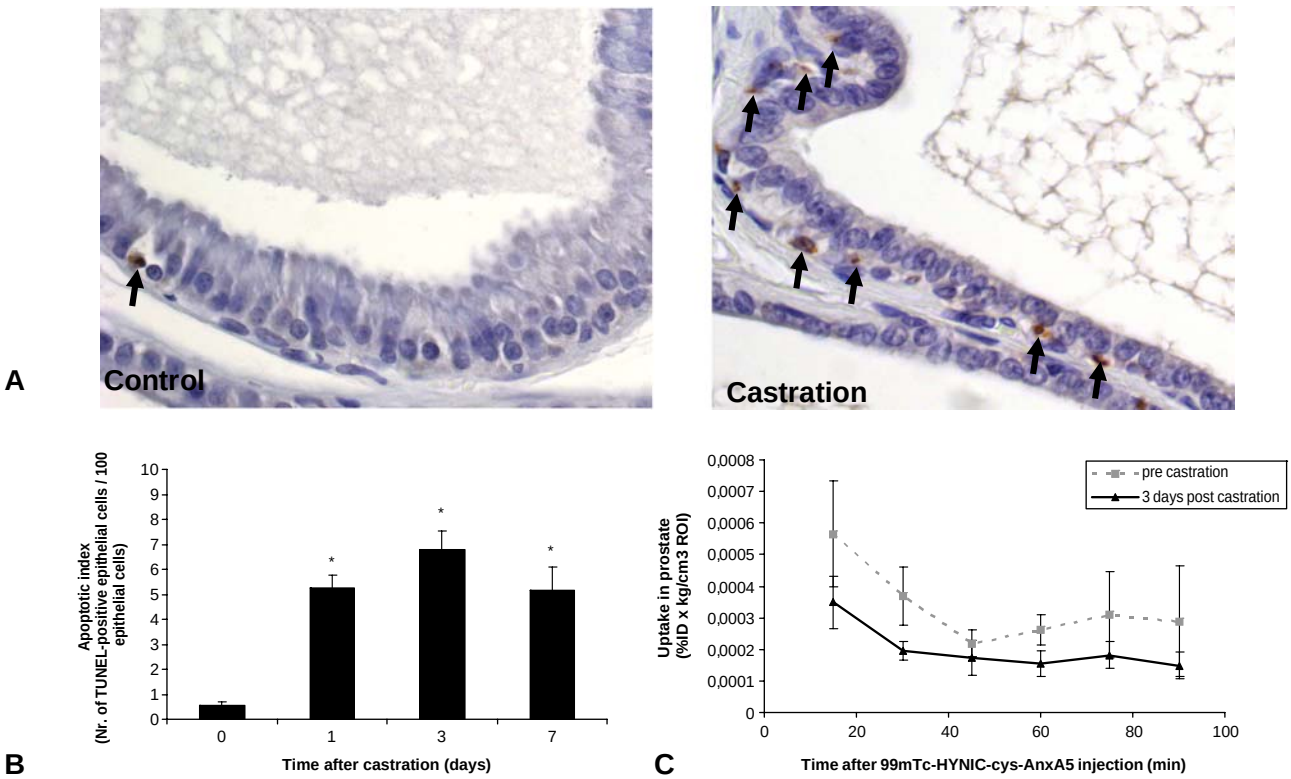

D

Post-mortem analysis	Uptake in prostate (%ID x kg/g)	Activity present in blood (%ID x kg/g)	Prostate : blood ratio
pre castration	0.020 +/- 0.001	0.012 +/- 0.003	1.9 +/- 0.6
3 days post castration	0.028 +/- 0.005	0.028 +/- 0.007	1.1 +/- 0.1

Fig. 6. **A** Representative microphotographs of TUNEL-stained sections of ventral prostates from a control and a castrated rat. Original magnification 200×. Arrows indicate apoptotic epithelial cells. **B** Apoptotic index of prostate epithelial cells at various times after castration (n= 3–4 animals per group). **C** Non-invasive SPECT assessment of ^{99m}Tc-HYNIC-cys-AnxA5 accumulation in the prostate of non-castrated rats or in the prostate of animals 3 days after castration (n=3–6 animals per group). **D** Post-mortem assessment of ^{99m}Tc-HYNIC-cys-AnxA5 uptake in the prostate, 210 min after tracer injection (n=2–3 animals per group). Data are expressed as mean +/− SEM. * indicates $p<0.05$ compared to control.

peripheral tissues (25–32). We now report that in a "deep" pharmacokinetic compartment like the prostate, despite high levels of cell death, no increase in annexin accumulation could be seen. A possible reason for this finding is the different tissue architecture between the prostate and the liver or spleen. Within the liver, apoptotic hepatocytes can be readily exposed to the circulating tracer, as a result of the fenestrated blood vessel endothelium. In our experiments as well as those of others (33,34), many TUNEL-positive cells observed in the liver during the early hours after cycloheximide exposure, appeared to be macrophages. These cells are readily accessible, given their convenient location at the luminal side of endothelial cells that delineate the sinusoids in the liver, while in spleen a similar situation is found. In contrast, capillary endothelial cells within the prostate are more tightly organized, with the main apoptotic cell type being situated behind this barrier. Moreover, apoptotic prostate epithelial cells are embedded in a layer of smooth muscle cells, fibroblasts and connective tissue that provide an additional barrier between the target cells and the circulation. The physicochemical characteristics of the tracer may, therefore, be critical factors in limiting passage of ^{99m}Tc-HYNIC-cys-AnxA5 across these barriers in the prostate, i.e. its molecular size preventing easy para-cellular transport, whereas its hydrophilicity also prohibits rapid trans-endothelial cell diffusion.

Yet, an alternative explanation for the lack of correlation between apoptosis and annexin uptake in the prostates of castrated rats should be considered. While castration induces prostate epithelial cell apoptosis, falling testosterone levels after ORX also result in a significant reduction of prostate perfusion (35,36). Although prostate perfusion was not measured in the current study, the uptake of annexin in prostates of castrated animals tended to be lower than in intact animals at all time points, which is in line with a reduction in perfusion taking place (Fig. 6C).

Considering the physiological and anatomical issues mentioned above, tracer pharmacokinetics will need to be optimized for imaging of cell death in the prostate to be successful. In Fig. 2, it can be seen that the distribution

clearance of ^{99m}Tc-HYNIC-cys-AnxA5 is very high. In general, the rapid clearance of a radiotracer is considered to be favorable, since it results in a rapid reduction of background signal originating from the blood. However, at the same time, such a rapidly declining plasma concentration limits the concentration-dependent drive behind tracer diffusion into peripheral compartments of the body. Maintaining high AnxA5 plasma levels for a longer period via a short-term i.v. infusion or injecting higher amounts of radio-labeled AnxA5 could, in principle, prolong the period available for an effective plasma concentration-driven diffusion of the tracer into peripheral tissues. The rapid decline in blood pool activity that can be expected after ending such an infusion period, combined with the high affinity binding of AnxA5 to PS residues on apoptotic/necrotic cells, may very well result in a selective retention of AnxA5 signal in the prostate. However, problems with regard to this approach are the increased exposure of the test subject to radiation, which concerns mainly the kidneys (37).

Bearing this in mind, it would prove interesting to examine lower dosages of small-molecule tracers with a higher degree of lipophilicity, yet with a similar affinity to PS residues or other cell death-selective markers. Diffusion of small lipophilic molecules into such tissues is likely to be less constrained by permeability issues, whereas a high affinity for PS or other cell death-selective markers should ensure retention when bound to target cells. The recently described 5-pyrrolidinylsulfonyl isatins for active caspase-3 labeling or ^{18}F-labeled 5-fluoropentyl-2-methyl-malonic acid may provide suitable small molecular candidates (38,39). With respect to ^{99m}Tc-AnxA5 SPECT imaging, our results suggest that applications will mainly be in the field of imaging cell death in organs in which apoptotic cells are separated from the circulation only by relatively loosely knit (endothelial cell) barriers and are relatively well-perfused. This includes imaging of cell death in tumor models, given the presence of dysfunctional angiogenic endothelium in many malignant tissues (40).

As a final point, the current study demonstrates that from a pharmacokinetic-methodological perspective, the SPECT/CT configuration used here is very well-suited for high-quality visualization of pharmacokinetics and biodistribution of radio-labeled proteins *in vivo*, even those with a very short distribution half-life. This illustrates that incorporation of non-invasive imaging techniques in the drug discovery process could indeed provide an elegant, alternative way of obtaining pharmacokinetic and biodistribution data of new chemical and biological entities.

CONCLUSIONS

The data presented in this paper demonstrate that accumulation of the novel annexin variant ^{99m}Tc-HYNIC-cys-AnxA5 correlates with increased levels of cell death in the macrophage populations of liver and spleen, induced by acute exposure to cycloheximide. In contrast, the increased apoptotic index observed in prostate epithelial cells following castration was not paralleled by an increase in annexin accumulation. These data suggest that additional optimization or alternative molecular probes may be required if apoptosis is to be successfully imaged in the prostate after castration. In contrast, the higher uptake of ^{99m}Tc-HYNIC-cys-AnxA5 in liver and spleen could be well-monitored via combined SPECT/CT imaging, demonstrating the utility of this annexin A5 variant for the non-invasive measurement of cell death in these organs. Such translational methods may prove useful in the characterization of disease processes, adverse drug-induced effects or development of new therapies targeting apoptosis.

ACKNOWLEDGEMENTS

C. van Kammen and C. van Helvert of the University of Maastricht are gratefully acknowledged for animal handling and experimentation, whereas R. van Brakel, M. Berben and S. Kivits are thanked for skillful conduction of the radiolabeling, biodistribution studies and SPECT/CT experiments, respectively. Finally, Drs. B. Henry, O. Steinbach, R. Rossin, C. P. Reutelingsperger, I. Verel, D. Attia, H. Hamersma and S. Addo are thanked for valuable scientific discussions.

REFERENCES

1. Rudin M, Weissleder R. Molecular imaging in drug discovery and development. Nat Rev Drug Discov. 2003;2:123–31.
2. Hargreaves RJ. The role of molecular imaging in drug discovery and development. Clin Pharmacol Ther. 2008;83:349–53.
3. Orsel JG, Schaeffter T. Molecular Imaging and applications for pharmaceutical R&D. In: Knäblein J, editors. Modern Biopharmaceuticals; 2005. pp. 1211–41.
4. Blankenberg FG. *In vivo* detection of apoptosis. J Nucl Med. 2008;49(Suppl 2):81S–95.
5. Boersma HH, Kietselaer BL, Stolk LM, Bennaghmouch A, Hofstra L, Narula J, et al. Past, present, and future of annexin A5: from protein discovery to clinical applications. J Nucl Med. 2005;46:2035–50.
6. Schlegel RA, Williamson P. Phosphatidylserine, a death knell. Cell Death Differ. 2001;8:551–63.
7. Fonge H, de Saint HM, Vunckx K, Rattat D, Nuyts J, Bormans G, et al. Preliminary *in vivo* evaluation of a novel 99mTc-labeled HYNIC-cys-annexin A5 as an apoptosis imaging agent. Bioorg Med Chem Lett. 2008;18:3794–8.
8. Schoemaker MH, Moshage H. Defying death: the hepatocyte's survival kit. Clin Sci (Lond). 2004;107:13–25.
9. Herr I, Schemmer P, Buchler MW. On the TRAIL to therapeutic intervention in liver disease. Hepatology. 2007;46:266–74.
10. Showalter SL, Hager E, Yeo CJ. Metastatic disease to the pancreas and spleen. Semin Oncol. 2008;35:160–71.
11. Greupink R, Reker-Smit C, Proost JH, Loenen Weemaes AM, de Hooge M, Poelstra K, et al. Pharmacokinetics of a hepatic stellate cell-targeted doxorubicin construct in bile duct-ligated rats. Biochem Pharmacol. 2007;73:1455–62.
12. Rijks LJ, van den Bos JC, van Doremalen PA, Boer GJ, de Bruin K, Doornbos T, et al. Synthesis, estrogen receptor binding, and tissue distribution of a new iodovinylestradiol derivative (17alpha, 20E)-21-[123I]Iodo-11beta-nitrato-19-norp regna-1, 3, 5 (10), 20-tetraene-3, 17-diol (E-[123I]NIVE). Nucl Med Biol. 1998;25:411–21.
13. Grierson JR, Yagle KJ, Eary JF, Tait JF, Gibson DF, Lewellen B, et al. Production of [F-18]fluoroannexin for imaging apoptosis with PET. Bioconjug Chem. 2004;15:373–9.
14. Yagle KJ, Eary JF, Tait JF, Grierson JR, Link JM, Lewellen B, et al. Evaluation of 18F-annexin V as a PET imaging agent in an animal model of apoptosis. J Nucl Med. 2005;46:658–66.
15. Boersma HH, Liem IH, Kemerink GJ, Thimister PW, Hofstra L, Stolk LM, et al. Comparison between human pharmacokinetics and imaging properties of two conjugation methods for 99mTc-annexin A5. Br J Radiol. 2003;76:553–60.
16. Haas M, de Zeeuw D, van Zanten A, Meijer DK. Quantification of renal low-molecular-weight protein handling in the intact rat. Kidney Int. 1993;43:949–54.

17. Birn H, Christensen EI. Renal albumin absorption in physiology and pathology. Kidney Int. 2006;69:440–9.
18. Haverdings RF, Haas M, Greupink AR, de Vries PA, Moolenaar F, de Zeeuw D, et al. Potentials and limitations of the low-molecular-weight protein lysozyme as a carrier for renal drug targeting. Ren Fail. 2001;23:397–409.
19. Tait JF, Smith C, Blankenberg FG. Structural requirements for *in vivo* detection of cell death with 99mTc-annexin V. J Nucl Med. 2005;46:807–15.
20. Hagens WI, Mattos A, Greupink R, Jager-Krikken A, Reker-Smit C, Loenen-Weemaes A, Gouw AS, Poelstra K, Beljaars L. Targeting 15d-Prostaglandin J(2) to Hepatic Stellate Cells: Two Options Evaluated. Pharm Res. 2007;24(3):566–74.
21. Blair JT, Thomson AW, Whiting PH, Davidson RJ, Simpson JG. Toxicity of the immune suppressant cyclosporin A in the rat. J Pathol. 1982;138:163–78.
22. Levine S, Gherson J. Morphologic effects of mitoxantrone and a related anthracenedione on lymphoid tissues. Int J Immunopharmacol. 1986;8:999–1007.
23. Olson H, Betton G, Robinson D, Thomas K, Monro A, Kolaja G, et al. Concordance of the toxicity of pharmaceuticals in humans and in animals. Regul Toxicol Pharmacol. 2000;32:56–67.
24. Navarro VJ, Senior JR. Drug-related hepatotoxicity. N Engl J Med. 2006;354:731–9.
25. Peker C, Sarda-Mantel L, Loiseau P, Rouzet F, Nazneen L, Martet G, et al. Imaging apoptosis with (99 m)Tc-annexin-V in experimental subacute myocarditis. J Nucl Med. 2004;45:1081–6.
26. Kuge Y, Sato M, Zhao S, Takei T, Nakada K, Seki KI, et al. Feasibility of 99mTc-annexin V for repetitive detection of apoptotic tumor response to chemotherapy: an experimental study using a rat tumor model. J Nucl Med. 2004;45:309–12.
27. Keen HG, Dekker BA, Disley L, Hastings D, Lyons S, Reader AJ, et al. Imaging apoptosis *in vivo* using 124I-annexin V and PET. Nucl Med Biol. 2005;32:395–402.
28. Murakami Y, Takamatsu H, Taki J, Tatsumi M, Noda A, Ichise R, et al. 18F-labelled annexin V: a PET tracer for apoptosis imaging. Eur J Nucl Med Mol Imaging. 2004;31:469–74.
29. Ke S, Wen X, Wu QP, Wallace S, Charnsangavej C, Stachowiak AM, et al. Imaging taxane-induced tumor apoptosis using PEGylated, 111In-labeled annexin V. J Nucl Med. 2004;45:108–15.
30. Mochizuki T, Kuge Y, Zhao S, Tsukamoto E, Hosokawa M, Strauss HW, et al. Detection of apoptotic tumor response *in vivo* after a single dose of chemotherapy with 99mTc-annexin V. J Nucl Med. 2003;44:92–7.
31. Corsten MF, Hofstra L, Narula J, Reutelingsperger CP. Counting heads in the war against cancer: defining the role of annexin A5 imaging in cancer treatment and surveillance. Cancer Res. 2006;66:1255–60.
32. Hofstra L, Liem IH, Dumont EA, Boersma HH, van Heerde WL, Doevendans PA, et al. Visualisation of cell death *in vivo* in patients with acute myocardial infarction. Lancet. 2000;356:209–12.
33. Ito K, Kiyosawa N, Kumagai K, Manabe S, Matsunuma N, Yamoto T. Molecular mechanism investigation of cycloheximide-induced hepatocyte apoptosis in rat livers by morphological and microarray analysis. Toxicology. 2006;219:175–86.
34. Kumagai K, Kiyosawa N, Ito K, Yamoto T, Teranishi M, Nakayama H, et al. Influence of Kupffer cell inactivation on cycloheximide-induced hepatic injury. Toxicology. 2007;241:106–18.
35. Ono Y, Suzuki K, Kashiwagi B, Shibata Y, Ito K, Fukabori Y, et al. Androgen-dependent blood flow control and morphological changes of the capillaries in rat prostate. Int J Androl. 2004;27:50–6.
36. Shibata Y, Kashiwagi B, Ono Y, Fukabori Y, Suzuki K, Honma S, et al. The evaluation of rat prostate blood flow using a laser speckle flowmetry: a comparative study using the microsphere method in castrated and androgen-replenished rats. Urol Res. 2004;32:44–8.
37. Kemerink GJ, Liem IH, Hofstra L, Boersma HH, Buijs WC, Reutelingsperger CP, et al. Patient dosimetry of intravenously administered 99mTc-annexin V. J Nucl Med. 2001;42:382–7.
38. Kopka K, Faust A, Keul P, Wagner S, Breyholz HJ, Holtke C, et al. 5-pyrrolidinylsulfonyl isatins as a potential tool for the molecular imaging of caspases in apoptosis. J Med Chem. 2006;49:6704–15.
39. Reshef A, Shirvan A, Waterhouse RN, Grimberg H, Levin G, Cohen A, et al. Molecular imaging of neurovascular cell death in experimental cerebral stroke by PET. J Nucl Med. 2008;49:1520–8.
40. Nagy JA, Benjamin L, Zeng H, Dvorak AM, Dvorak HF. Vascular permeability, vascular hyperpermeability and angiogenesis. Angiogenesis. 2008;11:109–19.